THE INFLUENCE OF TEXTILE ARCHITECTURE ON THE STRAIN-RATE DEPENDANT MATERIAL BEHAVIOUR OF CARBON FIBRE-REINFORCED COMPOSITES UNDER BENDING LOADING

W. A. Hufenbach[1], O. Renner[2], R. Bochynek[2*], A. Hornig[1]

[1]*Institute of Lightweight Engineering and Polymer Technology, Technische Universität Dresden, Holbeinstraße 3, 01307 Dresden, Germany*
[2]*Leichtbau-Zentrum Sachsen GmbH, Marschnerstraße 39, 01307 Dresden, Germany*
**corresponding author: ralph.bochynek@lzs-dd.de*

Keywords: carbon fibre-reinforced composites, textile architecture, strain-rate dependence, impact loading

Abstract
The strain rate dependent bending behaviour of carbon fibre-reinforced composites is investigated, whereby three different textile configurations such as a non-crimp fabric, a woven fabric and a triaxial braiding are considered. Experimental investigations have been performed at a servo hydraulic test system in combination with a high speed camera for optical at high strain rates. Finally, strain rate dependent material properties determined in bending tests and a phenomenologically based damage and failure analysis of the considered textile configurations are presented.

1 Introduction

Textile-reinforced composites offer in the field of high-performance materials the highest potential for being adapted to multiaxial load cases and complex components. Especially the material class of carbon fibre-reinforced composites combines low weight and high strength with good impact behaviour, what makes them quite attractive to applications in the aerospace industry. Nevertheless, the lack of trusted data and knowledge of damage and failure mechanisms under high-dynamic loading such as impact often leads to highly conservative design of structural components.

Due to very complex failure mechanisms in textile-reinforced composites [1-3] an adequate prediction of material behaviour after impact is still difficult, even if the strain-rate dependence of material data determined in coupon testing of unidirectional-reinforced composites is well known [4-5]. Since the specific textile architecture influences highly the mechanical behaviour of carbon fibre-reinforced composites, a very large number of additional tests are necessary to determine elastic and strength as well as damage and strain rate parameters for an adequate numerical modelling. The strain rate dependent in-plane and through thickness behaviour of textile-reinforced composites based on hybrid glass/polypropylene yarn has been investigated in detail experimentally and numerically [6-8]. Due to the large variety of different textile reinforcements and for reduction of experimental effort as well as costs, simple tests are required to determine the ability of different textile configurations for specific multiaxial load cases. A comprehensive comparative study regarding different textile reinforcement architectures is presented in [9].

Especially in aerospace applications, impact events with high loading velocities are common multiaxial load cases. By the detailed consideration of such an impact event, two dominating basic load cases are identified. Global bending and local through thickness shearing caused by the high-dynamic loading of an impactor are observed. For an estimation of the ability of different textile-reinforced composites for being used in impact structures, adapted testing rigs have to be designed to investigate the global bending and through thickness shearing behaviour. Experimental investigations of these basic load cases are performed with a bending and a puncture testing rig at a servo hydraulic high velocity test system. For conventional quantitative analysis of the experiments by force-displacement-curves, the force measurement system is located in the impactor to reduce the influence of oscillation of the testing rig while loading. For qualitative analysis of damage and failure behaviour of different textile-reinforced composites, a high speed camera system with a maximum frame rate of up to 200,000 images per second was used.
Within the scope of this work, the damage and failure behaviour after bending loading of conventional non-crimp fabric is compared with them of different textile architectures such as a woven fabric and a triaxial braiding. The quantitative and qualitative analysis shows a varying strain-rate dependence of each material configuration at the two considered load cases. From these results important conclusions on the ability for applications in impact structures can be drawn.

2 Experimental concept

2.1 Material configurations

Within the scope of this work, the influence of the textile architecture of carbon fibre-reinforced composites under bending on the strain rate dependent material behaviour is investigated. Here, the damage and failure behaviour after bending loading of conventional non-crimp fabric is compared with them of different textile architectures such as a woven fabric and a triaxial braiding. CT-scans of each textile configuration are presented in Figure 1.

Figure 1. CT-scans of textile configurations: non-crimp fabric (left), woven fabric (middle) and triaxial braiding (right)

Non-crimp fabrics are characterised by the straightened orientation of the roving. Due to the non-existence of crossing points in a single layer, mechanical properties such as stiffness and strength show the best possible performance. The poor compound between the rovings of a layer results in an insufficient drapability.
Woven fabrics are characterised by orthogonally crossed rovings. The large variety of different types of woven fabrics results in a wide range of mechanical and manufacturing properties. Compared to non-crimp fabrics, woven fabrics show a much better drapability.

The ondulation of the rovings causes decreasing mechanical properties. In this work a plain weave is investigated.
Braidings are characterised by the weaving of at least two roving systems to a piece. The angle between the crossing rovings can range from ±10° to ±80°. Additionally longitudinal rovings may be used to increase the mechanical properties in this direction. In this work a **triaxial braiding** with ±60° fibre orientation and straight rovings is considered.
The investigated material configurations consist of carbon fibre system TENAX HTS40 from TOHOTENAX. For consolidation the epoxy matrix system HEXFLOW® RTM 6 from HEXCEL was used, which is specifically developed for aerospace applications. The specimen panels have been manufactured by resin transfer moulding (RTM) [10]. Specimen preparation has been performed by waterjet cutting.

2.2 Testing setup

A servo hydraulic high velocity test system INSTRON VHS 160/20 has been utilised for the experiments. This rig enables tests at high deformation speeds of up to 20 m/s with a maximum force of 160 kN. Especially at high loading velocities, oscillations caused by the testing rig interact with the original loading measurement system located below the testing devices and may cause hardly analysable measurement data. Therefore, a new force measurement system has been developed, which is located inside the impactor. Forces are measured directly by strain gauges at the contact area between impactor and specimen, whereby the influence of oscillations on the force measurement is decreased significantly. Beside conventional force and displacement measurement the high speed camera system PHANTOM V7.2 with a maximum frame rate of up to 200,000 images per second was used for damage and failure analysis of the bending tests. An optical analysis of the through thickness tests is not possible due to the all-round fixture of the specimens.
Investigations of the bending behaviour have been performed with a 3-point bending device (see Figure 2). Load is applied with a straight fin with diameter of 5 mm and a length of 20 mm. Both supports of the testing device have a distance of 64 mm and a radius of 2 mm. The rectangular bending specimens have a length of 80 mm, a width of 20 mm and a thickness of 8 mm.

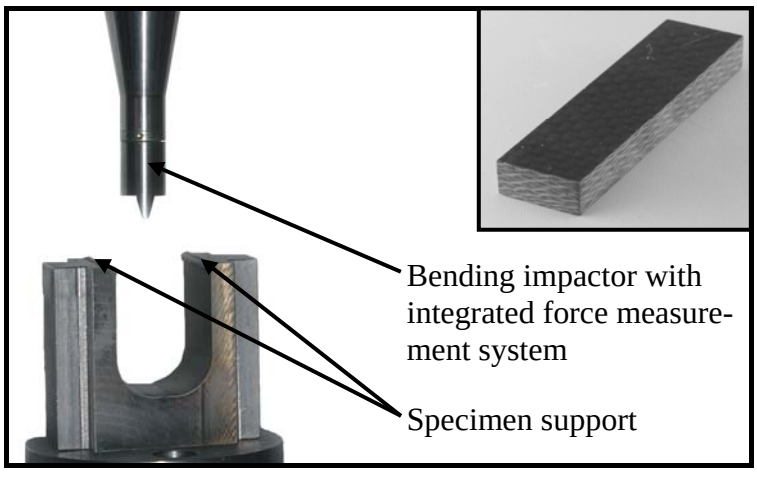

Figure 2. Testing rigs for experimental investigations: 3-point bending testing rig with rectangular specimen (left) and puncture testing rig with circular specimen (right)

Bending tests have been performed at 4 loading velocities for each textile configuration (see Table 1). With four repetitions per loading velocity and three material configurations a series of 48 experiments has been performed.
In these testing configurations conventional in-plane strain measurement with strain gauges has not been performed. Nominal strain rates of the 3-point bending tests have been calculated according DIN EN 2764 [11] with the following equation:

$$\dot{\varepsilon} = \frac{6 \cdot h \cdot v}{L^2} \tag{1}$$

where v is the loading velocity, L is the distance between both supports of the testing device and h is thickness of the specimens. The occurring strain rates for each textile configuration are analysed with equation (1) and presented in Table 1.

Material configuration	Loading velocities at bending tests [m/s]	Strain rates at bending tests [s^{-1}]
Non-crimp fabric	**4 decades** $9.4 \cdot 10^{-5}$; $9.7 \cdot 10^{-3}$; $9.0 \cdot 10^{-1}$; $5.9 \cdot 10^{0}$	**4 decades** $7.1 \cdot 10^{-3}$; $7.3 \cdot 10^{-1}$; $6.7 \cdot 10^{1}$; $4.4 \cdot 10^{2}$
Woven fabric	**4 decades** $9.4 \cdot 10^{-5}$; $9.6 \cdot 10^{-3}$; $8.7 \cdot 10^{-1}$; $6.0 \cdot 10^{0}$	**4 decades** $7.1 \cdot 10^{-3}$; $7.2 \cdot 10^{-1}$; $6.5 \cdot 10^{1}$; $4.5 \cdot 10^{2}$
Triaxial braiding	**4 decades** $9.5 \cdot 10^{-5}$; $9.5 \cdot 10^{-3}$; $8.8 \cdot 10^{-1}$; $6.1 \cdot 10^{0}$	**4 decades** $6.9 \cdot 10^{-3}$; $6.9 \cdot 10^{-1}$; $6.4 \cdot 10^{1}$; $4.5 \cdot 10^{2}$

Table 1. Overview of tested material configurations with loading velocities and strain rates

3 Experimental results and identification of material properties

3.1 Material behaviour and determination of material properties

Based on the discussed testing setup 4 force-displacement curves have been measured for each material configuration within each strain rate domain. Characteristic force-displacement curves in relation to the investigated material and testing configuration are illustrated in Figure 3 and Figure 4.

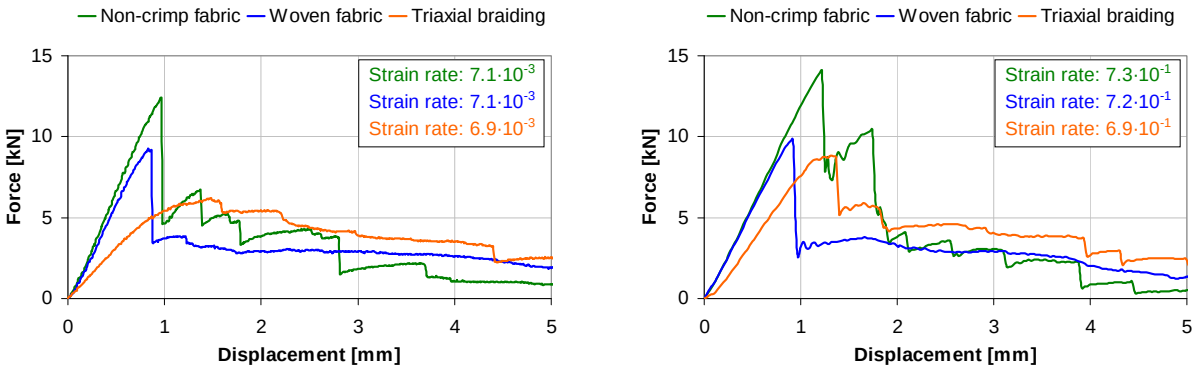

Figure 3. Characteristic force-displacement curves for the investigated material and testing configurations (lower strain rate domains)

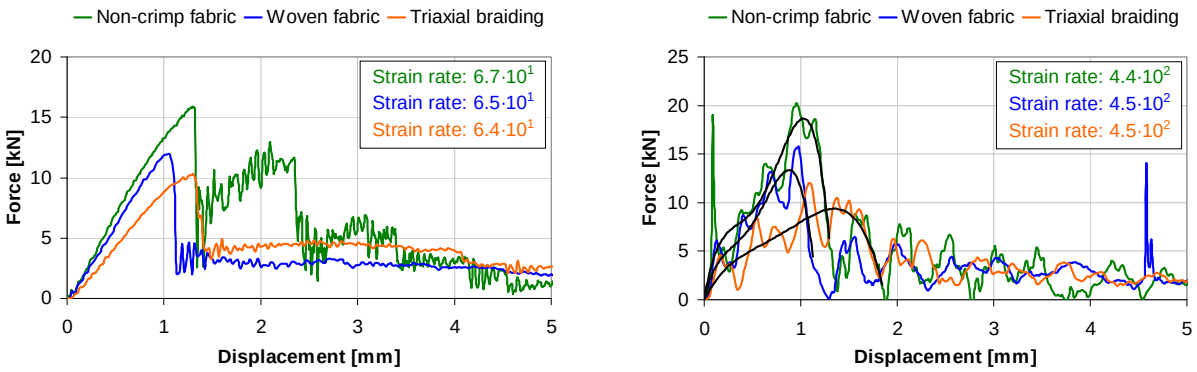

Figure 4. Characteristic force-displacement curves for the investigated material and testing configurations (higher strain rate domains)

In all investigated strain rate domains, the non-crimp and woven fabric show nearly the same slope of the force-displacement curve in the first loading steps, whereas the slope of the force-displacement curve of the triaxial braiding is lower.

For further analysis and identification of characteristic mechanical properties the maximum impact force F_M and the characteristic impact energy W_C is determined for all testing and material configurations. Maximum impact force is defined by the maximum of the force-displacement curve until significant decrease which is equivalent to failure of the specimen. Characteristic impact energy is defined by the area below the force-displacement curve until significant decrease (50 % of the maximum impact force) of the curve.

Due to large oscillations at the strain rate domain of $4.4 \cdot 10^2$ s^{-1}, force-displacement curves have been interpolated until the significant decrease and characteristic mechanical properties are determined from the analytical function.

The determined material parameters are arithmetically averaged over the number of tests and summarised in Table 2.

Material configuration	Strain rate [1/s]	Maximum impact force [kN]	Characteristic impact energy [J]
Non-crimp fabric	0.00707	12.283	6.308
	0.725	13.197	8.245
	67.369	15.488	11.448
	443.454	17.961	13.168
Woven fabric	0.00706	9.439	3.982
	0.717	9.852	4.746
	65.430	11.908	7.149
	446.777	12.821	8.486
Triaxial braiding	0.00691	7.147	7.633
	0.692	7.624	8.132
	64.300	9.090	9.042
	446.390	9.433	10.657

Table 2. Characteristic strain rate dependent material parameters

3.2 Strain rate dependence of material parameters

For exact quantitative comparison of the considered material configurations, the strain rate dependence is focused on the experimentally determined strength and energy parameters and was found to be accurately described within the experimental limits by the JOHNSON-COOK [12] based equation:

$$F_M(\dot{\varepsilon}) = F_M^{ref}\left[1 + A^F \ln\left(\frac{\dot{\varepsilon}}{\dot{\varepsilon}^{ref}}\right)\right] \quad \text{and} \quad W_C(\dot{\varepsilon}) = W_C^{ref}\left[1 + A^W \ln\left(\frac{\dot{\varepsilon}}{\dot{\varepsilon}^{ref}}\right)\right] \qquad (2)$$

In this equation F_M and W_C represent the maximum impact force and the characteristic impact energy of each material configuration at the current loading velocity $\dot{\varepsilon}$. The reference values F_M^{ref} and W_C^{ref} at a reference strain rate $\dot{\varepsilon}^{ref}$ and the material constants A^F and A^W describe the strain rate dependant behaviour of strength and energy parameters. It has to be emphasized, that equation (2) describes the material behaviour at least within the range of the experimentally investigated strain rate domains. A prediction of parameters outside of this range may results in unreasonable values.

An overview of the JOHNSON-COOK based model parameters for all material configurations is given in Table 3.

Testing configuration	**Material configuration**	$\dot{\varepsilon}^{ref}$ **[s^{-1}]**	F_M^{ref} **[J]**	W_C^{ref} **[J]**	A^F **[-]**	A^W **[-]**
Bending loading	Non-crimp fabric	0.00707	12.283	6.308	0.0345	0.0919
	Woven fabric	0.00706	9.439	3.982	0.0289	0.0910
	Triaxial braiding	0.00691	7.147	7.633	0.0281	0.0287

Table 3. Strain rate model parameters for the investigated material configurations

In Figure 5 the strain rate dependence of characteristic strength and energy parameters is presented. The experimentally determined values can be described accurately by the model parameters. With the help of these model parameters, it is possible to analysis the strain rate dependant bending behaviour of the investigated material configurations and to draw important conclusions on the ability of textile configurations for impact loaded structures.

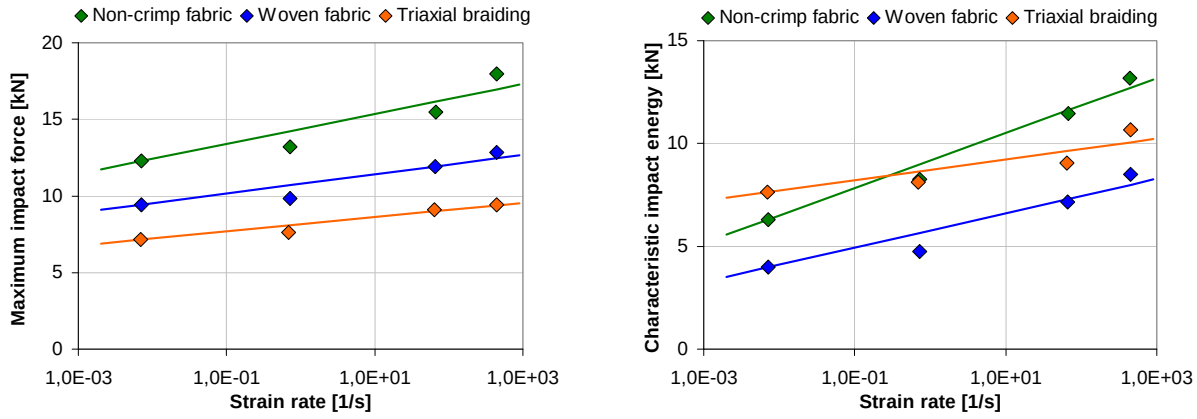

Figure 5. Strain rate dependence of characteristic material parameters

3.3 Phenomenologically based damage and failure analysis

For a detailed damage and failure analysis all tests have been recorded with the high speed camera system PHANTOM V7.2. Figure 6 to Figure 8 show recordings with 25,000 images per second of the material behaviour of a non-crimp fabric, a woven fabric and a trixial braiding at a loading velocity of ca. $9 \cdot 10^{-1}$ m/s.

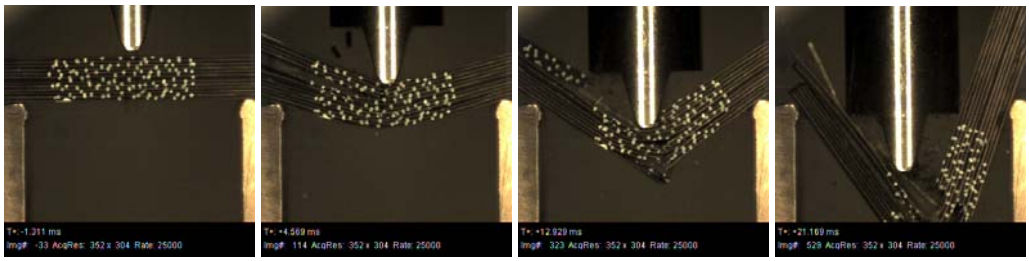

Figure 6. Damage and failure evolution of non-crimp fabric

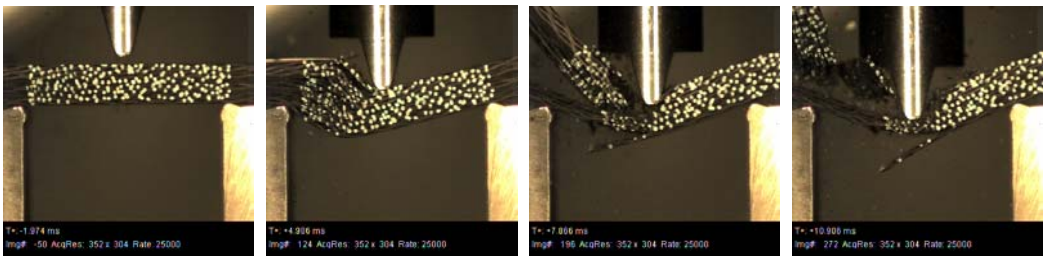

Figure 7. Damage and failure evolution of woven fabric

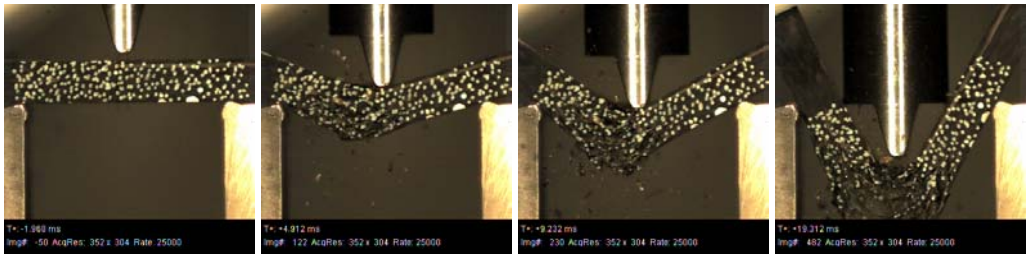

Figure 8. Damage and failure evolution of triaxial braiding

The non-crimp fabric specimen (Figure 6) show a very early, compared to the other material configurations, beginning of delamination between the single layers of the specimen. After catastrophic failure of the specimen nearly all layers of the specimen are separated and delaminated. The woven fabric (Figure 7) shows a similar behaviour but in a weakened form. Global delamination cannot be observed while loading the triaxial braiding (Figure 8) until failure. In the area of impact only slightly local delamination can be observed and the specimen is broken into two pieces.

4 Summary and conclusions

The strain rate dependant bending behaviour of carbon fibre-, textile reinforced composites has been investigated. High-dynamic bending tests have been performed with the three textile configurations non-crimp fabric, woven fabric and triaxial braiding. Testing results have been analysed with respect to characteristic strength and energy parameters and Johnson-Cook based model parameters have been determined to describe, compare and evaluate the strain

rate dependant material behaviour of the considered material configurations. Additionally, a phenomenologically based analysis of the damage and failure with a high-speed camera system has been performed. From these results important conclusions on the ability for applications in high dynamic loaded impact structures can be drawn. Besides that, further investigations should focus on the strain rate dependant through thickness shearing behaviour of different textile-reinforced composites to achieve a more detailed understanding of the phenomena of high-dynamic impact loading.

Acknowledgments

The authors wish to express their thanks for the financial support within the scope of the joint research project LEVITA. This project was supported with means of the European Regional Development Fund (ERDF) and the Free State of Saxony.

References

[1] Gerlach R., Siviour C. R., Wiegand J., Petrinic N.: In-plane and through-thickness properties, failure modes, damage and delamination in 3D woven carbon fibre composites subjected to impact loading. *Composites Science and Technology*, **Vol. 72**, pp. 397–411 (2012).

[2] Böhm R., Gude M., Hufenbach W.: A phenomenologically based damage model for 2D and 3D-textile composites with non-crimp reinforcement. *Materials and Design*, **Vol. 32**, pp. 2532-2544 (2011).

[3] Böhm R., Gude M., Hufenbach W.: A phenomenologically based damage model for textile composites with crimped reinforcement. *Composites Science and Technology*, **Vol. 70**, pp. 81–7 (2010).

[4] Sierakowsky R. L.: Strain rate effects in composites. *Applied Mechanics Reviews*, **Vol. 50**, pp. 741–761 (1997).

[5] Wang W., Makarov G., Shenoi R. A.: An analytical model for assessing strainrate sensitivity of unidirectional composite laminates. *Composite Structures*, **Vol. 69**, pp. 45–54 (2005).

[6] Hufenbach W., Hornig A., Zhou B., Langkamp A., Gude M.: Determination of strain rate dependent through-thickness tensile properties of textile reinforced thermoplastic composites using L-shaped beam specimens. *Composite Science and Technology*, **Vol. 71**, pp. 1110-1116 (2011).

[7] Hufenbach W., Gude M., Ebert C., Zscheyge M., Hornig A.: Strain rate dependent low velocity impact response of layerwise 3D-reinforced composite structures. *International Journal of Impact Engineering*, **Vol. 38**, pp. 358–368 (2011).

[8] Hufenbach W., Langkamp A., Hornig A., Zscheyge M., Bochynek R.: Analysing and modelling the 3D shear damage behaviour of hybrid yarn textile-reinforced thermoplastic composites. *Composite Structures*, **Vol. 94**, pp. 358–368 (2011).

[9] Hufenbach W., Böhm R., Thieme M., Winkler A., Mäder E., Rausch J., Schade M.: Polypropylene/glass fibre 3D-textile reinforced composites for automotive applications. *Materials and Design*, **Vol. 32**, pp. 121–131 (2011).

[10] Hufenbach W. (Ed.): *Textile Verbundbauweisen und Fertigungstechnologien für Leichtbaustrukturen des Maschinen- und Fahrzeugbaus*. Progress media-Verlag, Dresden (2007).

[11] DIN EN 2746. Luft- und Raumfahrt - Glasfaserverstärkte Kunststoffe - Biegeversuch - Dreipunktverfahren (1998).

[12] Johnson G. R., Cook W. H.: Fracture characteristics of three metals subjected to various strains, strain rates, temperatures and pressures. *Engineering Fracture Mechanics*, **Vol. 21 No. 1**, pp. 31-48 (1985).